Journal of Forestry Research (2025) 36:137
https://doi.org/10.1007/s11676-025-01929-5

ORIGINAL PAPER

How precise is precise enough? Tree crown segmentation using high resolution close-up multispectral UAV images and its effect on NDVI accuracy in *Fraxinus excelsior* L. trees

Lisa Buchner[1] · **Anna-Katharina Eisen**[1] · **Susanne Jochner-Oette**[1]

Received: 13 May 2025 / Accepted: 24 June 2025

Abstract Detailed individual tree crown segmentation is highly relevant for the detection and monitoring of *Fraxinus excelsior* L. trees affected by ash dieback, a major threat to common ash populations across Europe. In this study, both fine and coarse crown segmentation methods were applied to close-range multispectral UAV imagery. The fine tree crown segmentation method utilized a novel unsupervised machine learning approach based on a blended NIR–NDVI image, whereas the coarse segmentation relied on the segment anything model (SAM). Both methods successfully delineated tree crown outlines, however, only the fine segmentation accurately captured internal canopy gaps. Despite these structural differences, mean NDVI values calculated per tree crown revealed no significant differences between the two approaches, indicating that coarse segmentation is sufficient for mean vegetation index assessments. Nevertheless, the fine segmentation revealed increased heterogeneity in NDVI values in more severely damaged trees, underscoring its value for detailed structural and health analyses. Furthermore, the fine segmentation workflow proved transferable to both individual UAV images and orthophotos from broader UAV surveys. For applications focused on structural integrity and spatial variation in canopy health, the fine segmentation approach is recommended.

Keywords Leaf mass segmentation · Machine learning · Segment anything model · Ash dieback

Introduction

Remote sensing technologies provide powerful tools for surveying large-scale tree populations, enabling efficient, long-term monitoring of tree health and disease progression across broad landscapes. Unmanned aerial vehicles (UAVs) equipped with different sensor types have been proven to be suitable for the identification and monitoring of plant diseases in the context of various species (Torresan et al. 2017; Barbedo 2019). Disease-induced damage symptoms can often be detected through changes in reflectance within the visible and near-infrared (NIR) spectrum. Multispectral sensors mounted on UAVs are particularly well-suited for detecting diseased plants, offering high spatial resolution and the ability to capture subtle physiological changes across large areas (Zhang et al. 2019; Neupane and Baysal-Gurel 2021). Vegetation indices, derived from mathematical combinations of reflectance values across multiple wavelengths, are widely used to analyse spectral reflectance patterns. These indices provide valuable insights into plant physiological traits and are therefore important tools

Project funding: This study was conducted within the project FraxVir "Detection, characterisation and analyses of the occurrence of viruses and ash dieback in special stands of Fraxinus excelsior—a supplementary study to the FraxForFuture demonstration project" and receives funding via the Waldklimafonds (WKF) funded by the German Federal Ministry of Food and Agriculture (BMEL) and Federal Ministry for the Environment, Nature Conservation, Nuclear Safety and Consumer Protection (BMUV) administrated by the Agency for Renewable Resources (FNR) under grant agreement 2220WK40A4.

The online version is available at https://link.springer.com/.

Corresponding editor: Lei Yu

✉ Lisa Buchner
lbuchner@ku.de

[1] Physical Geography/Landscape Ecology and Sustainable Ecosystem Development, Catholic University of Eichstätt-Ingolstadt, 85072 Eichstätt, Germany

Published online: 09 October 2025

for detecting disease symptoms and monitoring vegetation health (Huete 2012). The Normalized Difference Vegetation Index (NDVI), which is based on the differential reflectance of red and near-infrared wavelengths by plant canopies, is one of the most commonly and effective vegetation indices for detecting plant stress, as it enables early detection of physiological responses to stressors (Neupane and Baysal-Gurel 2021).

An increasingly important application of remote sensing technologies is the detection and monitoring of ash dieback, a disease that poses a major threat to European forest ecosystems. Since the introduction of the invasive fungal pathogen *Hymenoscyphus fraxineus* (Baral et al. 2014) in Europe and the first disease reports in Poland in the 1990s, ash dieback has severely affected populations of European common ash (*Fraxinus excelsior* L.). The fungal pathogen produces airborne ascospores that primarily infect leaves (Timmermann et al. 2011), initially causing necrotic lesions on leaflets and rachises. From there, the infection spreads into twigs and shoots, leading to branch dieback, wilting, and necrotic bark lesions, especially in young tissues. Eventually, the infection progresses into larger branches and stems, resulting in crown dieback characterised by extensive leaf loss (Gross et al. 2014; Timmermann et al. 2017; Fuchs et al. 2024). In advanced stages, necroses may also develop at the stem base, further weakening the tree (Langer 2017). This disease trajectory, from initial leaf infection to full crown dieback, can vary in speed depending on environmental conditions, tree age, and genetic resistance, but often results in high mortality within a few years after the onset of visible symptoms (Timmermann et al. 2017; Klesse et al. 2021). The European common ash is ecologically vital, supporting numerous dependent species (Mitchell et al. 2017; Hultberg et al. 2020) and is expected to experience severe population declines across Europe in the coming decades due to ash dieback (Coker et al. 2019). Therefore, efforts to identify, monitor and characterise affected ash trees are crucial for the long-term conservation of this ecologically important species.

The application of remote sensing technologies for assessing ash tree health remains limited. Some research has focused on monitoring damage caused by the emerald ash borer (*Agrilus planipennis*), a major insect pest threating ash populations, analysing hyperspectral (Pontius et al. 2008) and satellite data (Murfitt et al. 2016). Hyperspectral data have also been successfully used to identify ash trees damaged by ash dieback (Chan et al. 2021; Polk et al. 2022). The more frequently available multispectral data and the thereof calculated vegetation indices have been used to identify and segment ash tree crowns in a mixed forest and subsequently to classify the damage caused by ash dieback (Waser et al. 2014). Kampen et al. (2019) likewise analysed multispectral UAV data and successfully segmented ash tree crowns and characterised ash dieback severity. A different approach was taken by Flynn et al. (2024), who analysed 3D RGB point cloud data from UAV surveys of individual ash trees regarding the different internal crown greenness patterns of trees with differing degrees of damage. Furthermore, Buchner et al. (2025) examined vegetation index values across different damage classes using both RGB and multispectral data, identifying clear value ranges distinguishing mildly from severely affected trees. However, while Buchner et al. (2025) manually delineated ash tree crowns to only analyse leaf mass, no study to date has focused on automatically segmenting ash tree crowns from their surroundings to exclusively study the leaf mass in relation to ash dieback. As the crown of severely affected ash trees decreases drastically and typically presents multiple crown gaps, the exclusion of ground pixels is crucial for the accuracy of further analysis.

Multiple approaches for tree crown segmentation have been successfully developed utilising a wide range of different data, including airborne laser scanning (Dalponte et al. 2015; Argamosa et al. 2016; Douss and Farah 2022), hyperspectral data (Dalponte et al. 2015), satellite data (Lassalle et al. 2022), as well as RGB (Mohan et al. 2017; Huang et al. 2018; Tahar et al. 2021) and multispectral data (Qiu et al. 2020; Ulku et al. 2022). These diverse datasets support a broad spectrum of tree crown delineation techniques, ranging from traditional methods such as valley following, region growing or marker-controlled watershed segmentation to more recent machine and deep learning models (Ke and Quackenbush 2011; Kestur et al. 2018; Freudenberg et al. 2022; Zheng et al. 2025). While tree crown segmentation has been widely explored, the focus in many studies often lies in detecting and counting individual trees rather than on analysing the structural or physiological condition of the crown itself (Ke and Quackenbush 2011; Zheng et al. 2025). Nevertheless, segmentation precision is essential in downstream tasks such as disease detection, where accurate delineation of crown boundaries and internal features become critical.

This study, therefore, investigated two approaches for segmenting tree crowns, producing both fine and coarse tree crown masks, to assess whether the choice of segmentation method significantly affects the calculation of mean NDVI. In addition, we examined how varying levels of crown damage influence the spatial homogeneity of NDVI values within individual tree crowns.

Materials and methods

Study sites

This study was conducted in 2023 at two ash seed orchards in the federal state of Baden-Wuerttemberg, located in

southern Germany (Fig. 1). Both sites have already been included in previous studies on ash dieback (Enderle et al. 2015, Buchner et al. 2022, Eisen et al. 2022, 2023, 2024; Buchner et al. 2024, 2025).

The first site, the Emmendingen orchard (48° 7′ N, 7° 52′ E, 210 m a.s.l.) is situated about 15 km north of Freiburg. Covering 2.7 ha, this plantation was established in 1995 with an initial layout of 228 ash trees planted in a 10 m × 10 m grid. While no thinning operations were conducted, many trees had to be removed due to the impact of ash dieback. The site also contains a variety of other tree and shrub species growing close to the ash trees.

The second site, the Schorndorf orchard (48°46′ N, 9°25′ E, 420 m a.s.l.), lies east of Stuttgart, the capital of Baden-Wuerttemberg. It was established in 1992 with an original planting density of 7 m × 7 m, spanning approximately 2.27 ha. Initially, 416 ash trees were planted, but over time, more than half of them have been removed as a result of both thinning measures and the effects of ash dieback. Additional tree species, such as fruit trees, are also present on the orchard.

For the close-up UAV images, 30 ash trees were selected at each study site. These trees were evenly distributed throughout the orchards, exhibiting varying degrees of ash dieback symptoms, from mild to very severe symptoms.

Vitality assessment

Each selected tree was individually assessed for its vitality status in the field at the end of July 2023. Using a vitality scoring system (Peters et al. 2021) trees were classified based on their visible damage symptoms. Due to the widespread presence of ash dieback in Germany (Fuchs et al. 2024), no completely healthy trees were found at either of the two ash seed orchards. Consequently, the healthy tree category (class 0) was omitted. Trees with mild damage symptoms were assigned to classes 1 and 2, while those with severe damage symptoms were classified as classes 3 and 4. Dead trees (class 5) were not relevant to our study. Each damage class was defined by multiple criteria, including leaf loss, the percentage of dead shoots and branches, the presence of epicormic shoots and stem rot necrosis, with increasing symptom severity from class 1 to class 4.

Image acquisition

Close-up UAV images

For both study sites, individual close-up images of the 30 selected ash tree crowns were recorded using the UAV system DJI Mavic 3 Multispectral (Mavic 3 M) during June, July and October 2023. The Mavic 3 M is equipped with a 20 MP RGB camera and four 5 MP multispectral sensors, allowing for simultaneous capture of both RGB and multispectral images. The multispectral sensors cover four wavelength bands: NIR (860 nm ± 26 nm), red edge (730 nm ± 16 nm), red (650 nm ± 16 nm), and green (560 nm ± 16 nm). Additionally, an integrated sun sensor measures solar radiation to enable light compensation during post-processing (DJI 2022).The images were captured at an altitude of approximately 8 m above the tree crowns,

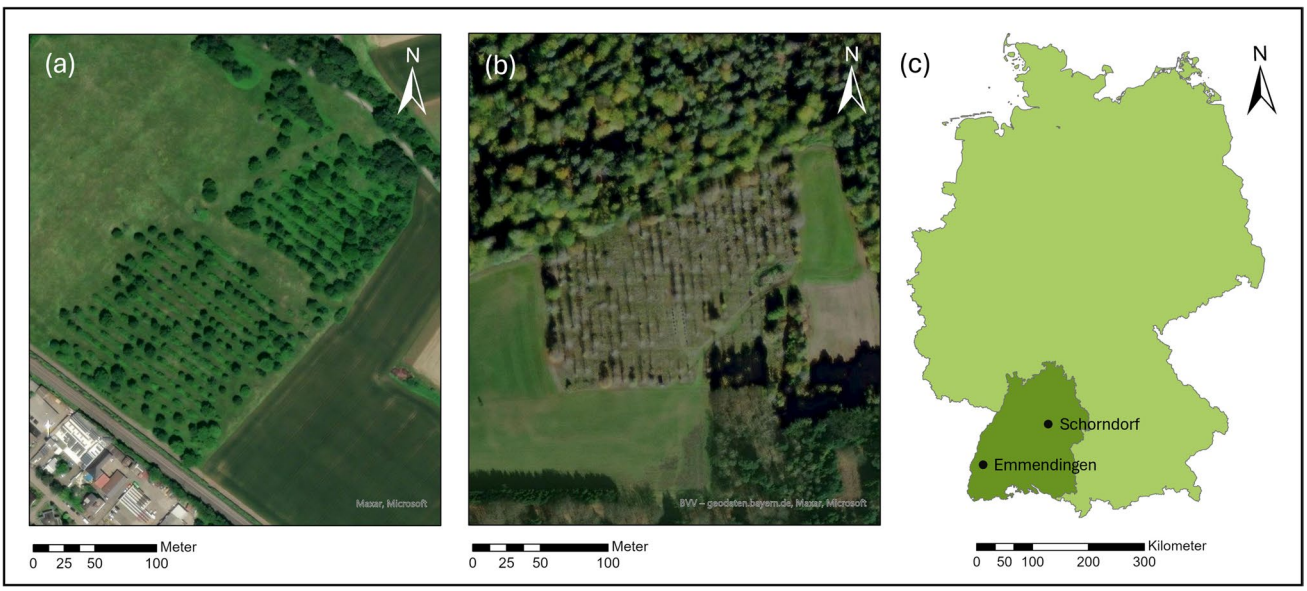

Fig. 1 Study sites Emmendingen (**a**) and Schorndorf (**b**) in the federal state of Baden-Wuerttemberg (dark green) in Germany (**c**, light green), *Source*: Esri Base Map, BKG 2025dl-de/by-2-0

providing an exceptionally high spatial resolution that ensures detailed image quality.

UAV survey

Additionally, a UAV survey was conducted at the Schorndorf orchard in July 2023 at a flight altitude of 80 m to further test the newly developed tree crown segmentation method. The Mavic 3 M followed a pre-planned flight plan with 85% front and side overlap and a flight speed of 4 m/s. This ensured a ground sampling distance of 2.77 cm/pixel for the captured multispectral images. The survey was divided into two flight missions, due to the size of the plantation and UAV specific battery capacity. However, the missions were conducted back-to-back to minimize variations in the environmental conditions.

The images were georeferenced using the integrated RTK data and processed into an orthophoto by aligning the images and generating a point cloud using the software Agisoft Metashape Professional (version 1.8.1).

Post-processing of the close-up UAV images

Due to the slight spatial offset between the four built-in multispectral sensors in the UAV system, the individual close-up images captured by each sensor were not perfectly aligned, resulting in minor misregistration between spectral bands. As a result, precise image alignment was required prior to further processing. Using a custom-built Python (version 3.13.0) script, the NIR, red edge, and red band images were co-registered to the green sensor image for each capture, which served as the reference. The applied homography-based image registration algorithm implemented in OpenCV aligned the images by calculating a 3×3 transformation matrix that mapped matching points from the non-reference images to the green reference image. Throughout the co-registration process, the original metadata of the images was retained.

Tree crown segmentation

Two different methods of individual tree crown segmentation were applied, creating a coarse and a fine mask for each tree crown. While the coarse mask was designed to capture the general outline of the tree crown, the fine mask aimed to incorporate the detailed crown structure, including internal gaps and irregularities.

To extract the coarse tree crown masks from UAV-based imagery, we applied the pre-trained Segment Anything Model (SAM) (Kirillov et al. 2024), a general-purpose segmentation framework developed for prompt-driven object segmentation, using a custom-built Python (version 3.11.0) script. SAM features a modular architecture consisting of an image encoder, a prompt encoder, and a mask decoder. The image encoder converts the input image into a latent representation capturing spatial and semantic features. User-provided prompts are processed by the prompt encoder and guide the segmentation process. Finally, the mask decoder integrates both embeddings to produce one or more segmentation masks (Kirillov et al. 2024; Speckenwirth et al. 2024). In this study, grayscale NIR images were converted to 3-channel grayscale RGB images to match the input format expected by the model. A single foreground point was manually placed near the centre of each image to indicate the approximate location of the tree crown. Based on this input, multiple candidate masks were generated by SAM. Each mask was visually assessed, and the most accurate one representing the crown shape was selected and exported as a binary mask for further analysis.

The fine tree crown masks were generated using a custom-built R (version 4.1.1) script, executed in R Studio (version 2021.09.0). The script integrated spectral, textural, and edge-based features into a multistep segmentation workflow comprising image preprocessing, feature extraction, unsupervised clustering, and morphological refinement (Fig. 2). First, the NIR and red bands were normalized to a range of 0–1, and the NDVI was computed as follows:

$$NDVI = \frac{NIR - Red}{NIR + Red} \quad (1)$$

To enhance vegetation signals, a hybrid image was constructed using a weighted combination of NDVI and NIR, assigning a weight of 0.4 to NDVI and 0.6 to NIR:

$$Hybrid\ image = 0.4 * NDVI + 0.6 * NIR \quad (2)$$

The hybrid image was subsequently normalized and enhanced using histogram equalization based on the empirical cumulative distribution function (ECDF) to improve local contrast. To characterize spatial structure, texture metrics (contrast, entropy, mean, and variance) were calculated from the equalized hybrid image using a grey level co-occurrence matrix (GLCM) with a 5×5 moving window. In addition, edge features were extracted using the Sobel operator by computing gradient magnitudes in both horizontal and vertical directions to enhance boundary detection. All derived features were compiled into a multilayer raster stack, providing a comprehensive representation of spectral, textural, and structural scene characteristics. Pixel-level values were extracted into a data frame and subjected to k-means clustering with $k = 2$, using Euclidean distance and random initialization. The cluster most representative of vegetation was identified by selecting the one with the highest mean texture value, and a corresponding binary mask was generated. To improve segmentation accuracy, morphological post-processing was applied. Small gaps within the

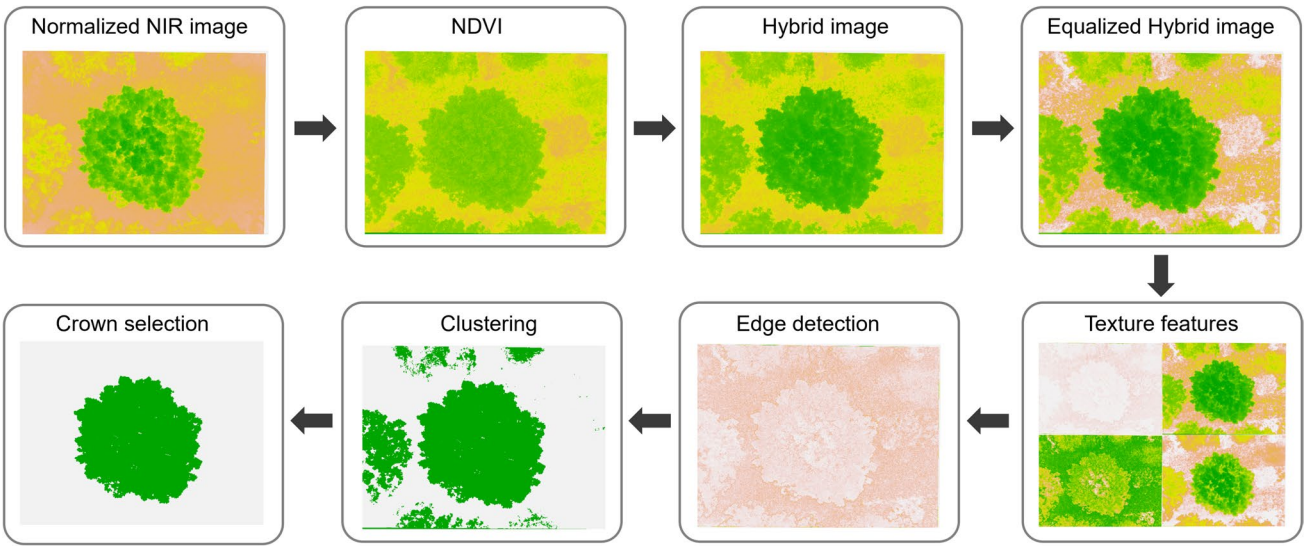

Fig. 2 Workflow for segmenting a fine tree crown mask

crown mask were filled using a 3 × 3 maximum filter, and boundaries were smoothed using a 3 × 3 mean filter. Pixels with smoothed values greater than 0.5 were retained in the final binary mask. To select only the tree crown, a minimum size threshold of 900 pixels was applied. The resulting mask constitutes a spatially constrained and structurally refined representation of the tree crown.

Each segmented fine and coarse tree crown mask was visually validated with the RGB image of the tree crown. Additionally, two sections from two different tree crowns were chosen and manually segmented. Due to the required level of segmentation detail, not all trees were segmented manually; only a representative subset of twelve trees in total, three typical trees per vitality class, was selected for validation. In ArcGIS Pro (version 2.8.3), the manual segmentation was executed, and a tree crown polygon was generated for all three mask types: manual, fine and coarse. The total area was calculated for all masks. To quantify the overlap between the segmentations, we employed the *Intersect* tool to create an intersection polygon (Area_overlap), for both the comparison of the manual and automated fine and coarse segments. This allowed to compute the Intersection over Union (IoU), a widely used metric for segmentation accuracy (Mishra et al. 2021; Sahin et al. 2023; Speckenwirth et al. 2024). The IoU is defined as the ratio of the overlapping area between the manual segmentation (A) and the automated segmentation masks (B) to the total area encompassed by both, as defined by Eq. 3.

$$\mathrm{IoU} = \frac{A \cap B}{A \cup B} \tag{3}$$

In addition to IoU, we examined false positives and false negatives to identify over- and under-segmentation. The *Erase* tool in ArcGIS Pro was used to extract false positives, representing areas detected by the automated segmentations but absent in the manual delineation. False negatives, on the other hand, represent regions that were included in the manual segmentation but missed by the automated methods. To further evaluate segmentation performance, Precision and Recall were computed, as shown in Eqs. 4 and 5:

$$Precision = \frac{Area_{overlap}}{Area_{overlap} + Area_{falsepositive}} \tag{4}$$

$$Recall = \frac{Area_{overlap}}{Area_{overlap} + Area_{falsenegative}} \tag{5}$$

Based on these, we derived the F1-score as described by Eq. 6, which highlights the correctly identified true positives and true negatives:

$$F1score = 2 \times \frac{Precision * Recall}{Precision + Recall} \tag{6}$$

As an additional test, the novel fine tree crown segmentation workflow was applied to the orthophoto of the Schorndorf orchard. Following the generation of a binary tree crown mask, the output was spatially aligned with the georeferenced tree positions recorded using the Stonex S9III (STONEX® Srl, Paderno Dugnano, Italy). This alignment enabled the integration of the segmentation results with precise ground-truth coordinates.

Statistical analysis

For both fine and coarse segmented tree crown masks, a mean NDVI value was calculated. To assess differences in the mean values and standard deviation (SD) of NDVI values between the fine and coarse mask types across vitality classes, pairwise statistical comparisons were conducted using the Wilcoxon rank-sum test.

To assess differences between the coarse and the fine tree crown segmentations, the proportion of crown area differences between the two mask types was quantified. Since tree crowns vary in size, direct comparisons of absolute differences would be misleading. Therefore, the difference area was expressed as a proportion of the total coarse mask area, ensuring an unbiased comparison across trees of different sizes. The resulting proportionate difference values were analysed in relation to tree health classifications to identify potential differences in segmentation refinements across different vitality conditions.

Additionally, only the NDVI values of the fine mask were further analysed to assess the homogeneity of index values per tree crown in relation to vitality class. Both the SD and coefficient of variation (CV) were calculated per tree crown and tested for statistical differences between the four vitality classes. A Kruskal–Wallis test was performed to determine whether significant variation existed between vitality classes. Post-hoc pairwise comparisons were conducted using the Wilcoxon rank-sum test with Bonferroni correction.

Results

Segmentation results and evaluation

Both methods applied for the automatic segmentation of ash tree crowns successfully identified and delineated the crown shape, as illustrated in Fig. 3, which shows four exemplary ash trees representative of the four vitality classes analysed

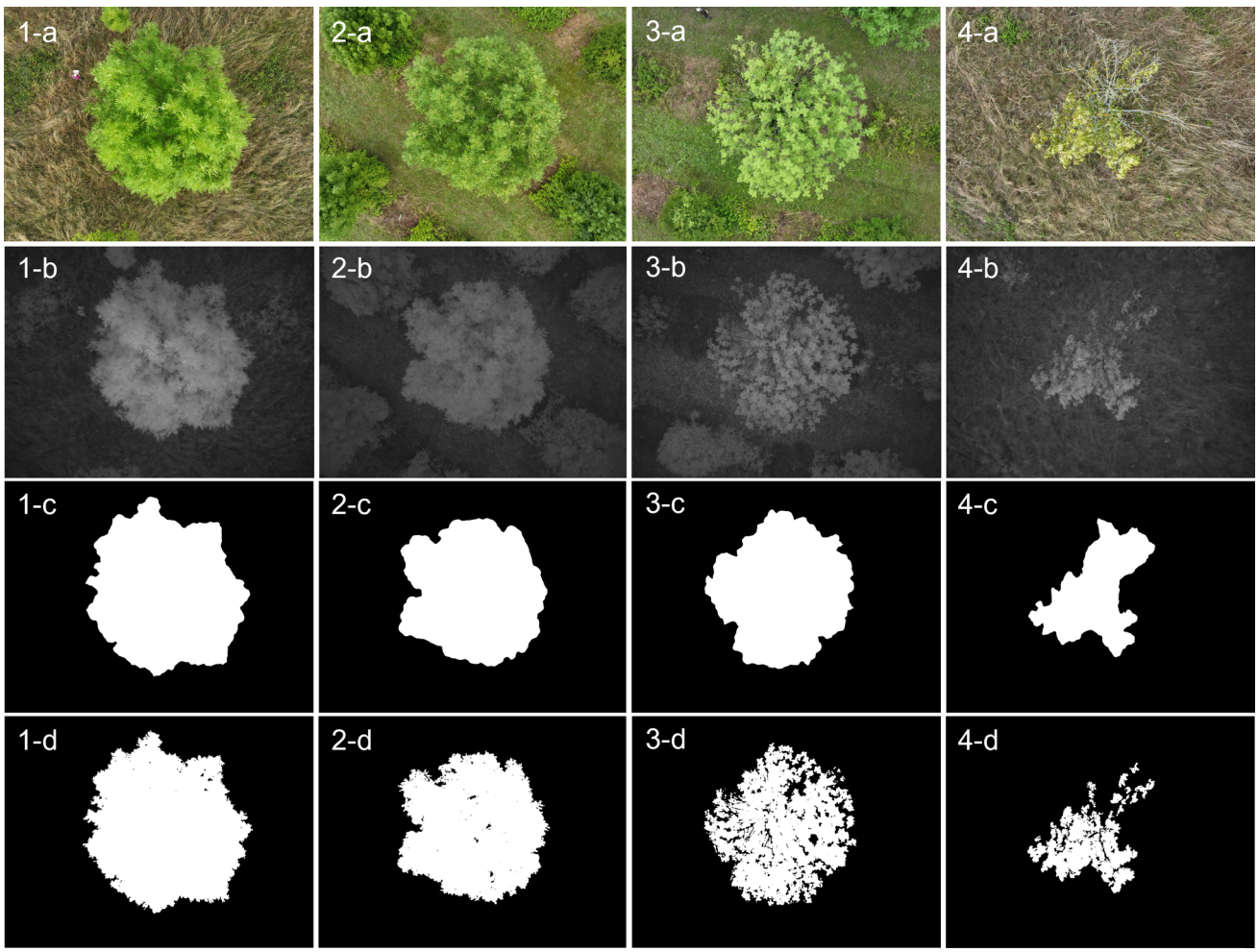

Fig. 3 RGB image (**a**), NIR image (**b**), coarse mask (**c**) and fine mask (**d**) of four exemplary ash tree crowns for the four vitality classes 1 to 4

in this study. The coarse mask worked well for trees with only mildly damage (Fig. 3: 1-c and 2-c). However, for trees with more severe damage, crown gaps were not sufficiently considered (Fig. 3: 3-c and 4-c). Particularly for trees with very severe damage (vitality class 4) large areas of ground pixels were included in the coarse crown mask. In comparison, the fine mask was able to segment the leaf mass in more detail, especially for the more severely damaged trees (Fig. 3: 3-d and 4-d). While segmentation results from the fine and coarse masks were visually similar for trees in vitality classes 1 and 2, the fine mask provided a more precise representation of the crown for trees in classes 3 and 4.

All 360 segmented tree crown masks were validated visually in comparison with the RGB images. Six individual trees, three of the coarse and three of the fine masks did not accurately segment the tree crown. Consequently, both mask types for these six trees were subsequently excluded from further analysis.

To systematically evaluate the segmentation performance across varying crown conditions, the fine and coarse segmentation masks were compared to manually delineated reference crowns across four vitality classes (Table 1). Both masks achieved high IoU values (mean IoU of 0.94 for the fine and 0.93 for the coarse mask). The manually segmented mask accurately represented internal gaps, while the coarse mask did not present any crown gaps. As a result, even over-segmented crowns, such as those from the coarse mask, could still achieve a high IoU due to increased overlap with the manual reference crown. Nevertheless, differences between the fine and coarse mask emerged in the precision and F1-score, particularly under more structurally heterogeneous conditions for trees with severe damage due to ash dieback. Both mask types were able to capture the outline of the crown (Fig. 4c, d), however while the fine mask was able to represent internal crown gaps in high detail, the coarse mask only captured the outline of the crown (Fig. 4g, h). The fine mask exhibited consistently higher accuracy across most metrics. Notably, in vitality class 4, representing crowns with severe damage and increased structural irregularity, the fine mask substantially outperformed the coarse mask in terms of precision (0.86 vs. 0.78) and F1-score (0.91 vs. 0.85), indicating an increased ability to avoid over-segmentation in complex canopy structures. While both mask types achieved similarly high recall values across all vitality classes (≥ 0.97), reflecting a general robustness in detecting crown presence, the fine mask demonstrated greater consistency and balance across all evaluated metrics. The overall higher precision (0.94 vs. 0.91) and F1-score (0.96 vs. 0.94) of the fine mask further underscore its enhanced delineation quality. These results suggest that increased spatial detail in

Table 1 Mean investigated metrics to evaluate the success of segmentation of the fine and coarse mask in comparison the manual segmentation (ground truth) for the four vitality classes, each class represented by three individual trees

Class	Ground truth—fine mask				Ground truth—coarse mask			
	IoU	Precision	Recall	F1	IoU	Precision	Recall	F1
Class 1	0.97	0.98	0.99	0.98	0.96	0.99	0.98	0.98
Class 2	0.95	0.96	0.99	0.98	0.93	0.96	0.98	0.97
Class 3	0.92	0.97	0.95	0.96	0.89	0.92	0.97	0.95
Class 4	0.93	0.86	0.98	0.91	0.94	0.78	0.97	0.85
Overall mean	0.94	0.94	0.98	0.96	0.93	0.91	0.97	0.94

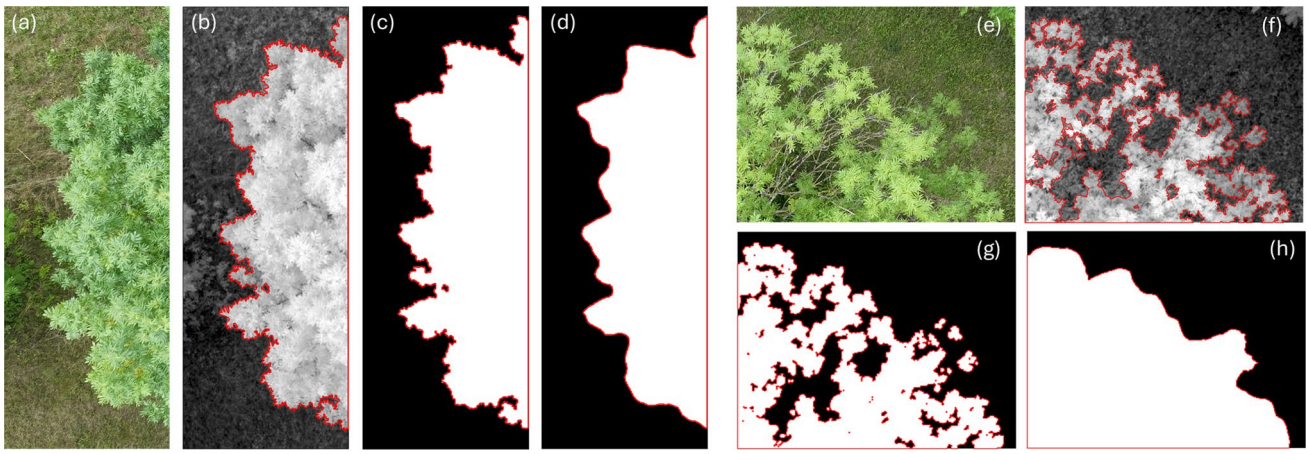

Fig. 4 RGB image (**a**, **e**), detailed manual segmentation of a part of a tree crown (**b**, **f**), fine segmentation (**c**, **g**) and coarse segmentation (**d**, **h**) of the edge area of an ash tree crown (**a**–**d**) and a crown with severe gaps (**e**–**h**)

crown segmentation enhances accuracy, particularly under conditions of elevated canopy heterogeneity.

Differences per mask type

Based on the 174 individual images of analysed ash trees derived from the different flight missions in June, July and October from both ash orchards, slightly higher NDVI values were recorded for the fine mask in comparison to the coarse mask. However, these differences were not statistically significant in any of the four vitality classes (Fig. 5). Independent from the mask type, a decrease in NDVI values was observed with an increasing damage due to ash dieback. Additionally, the mean NDVI calculated for the difference area (the region included in the coarse mask but excluded in the fine mask) was significantly lower than that of the fine mask in all vitality classes ($p < 0.001$), indicating that the excluded areas, mainly ground pixels beneath the crown and large exposed branches, have substantially lower NDVI values.

In contrast to the mean NDVI results, the SD values differed between the fine and coarse mask, with a significant difference observed between mask types in both vitality classes 2 and 3 (Fig. 5). The SD of the NDVI values increased with vitality class, demonstrating greater variability in NDVI values for severely damaged ash tree crowns.

The proportionate difference area between the coarse and fine mask, demonstrated an increase with more severely damaged ash trees (Fig. 6). The Kruskal–Wallis test proved statistical significance ($p = 0.022$). While the area between the two mask types differed only slightly for class 1, the difference was much more pronounced in classes 3 and 4, indicating differing fine and coarse segmentations. The post-hoc test revealed a statistically significant difference only for class 1 and 3 ($p = 0.033$). However, these results indicate an increasing deviation of the segmented areas of the two mask types with increasing damage severity, likely attributable to the increase of crown gaps with more severe damage.

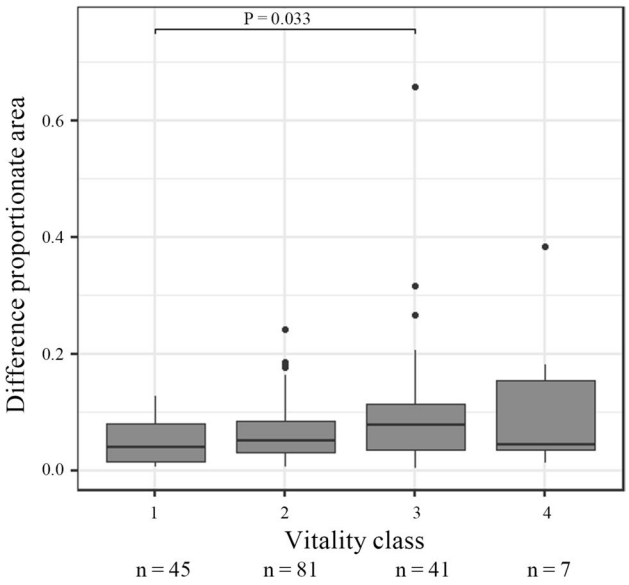

Fig. 6 Difference proportionate area between coarse and fine masks for the four vitality classes for the analysed 174 images from ash trees at the two seed orchards

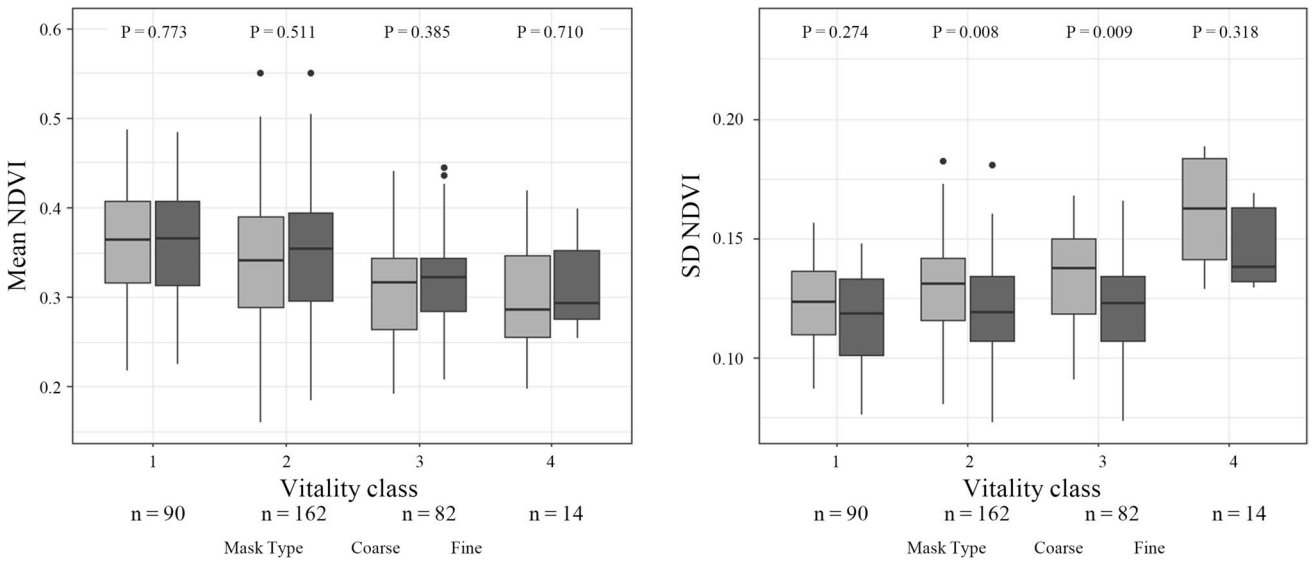

Fig. 5 Boxplots of the mean and SD NDVI values calculated from the two mask types, analysed among the 174 images for both coarse and fine masks, for the four vitality classes at the two seed orchards

Homogeneity of NDVI values

To assess spatial variability of NDVI in relation to canopy condition, the SD and CV of NDVI values were calculated for individual trees applying the fine crown segmentation method and compared across vitality classes (Fig. 7). Boxplot analysis revealed a significant increase in both NDVI SD (Kruskal–Wallis, p-value = 0.024) and NDVI CV (Kruskal–Wallis, p-value = 0.012) with declining tree vitality. Notably, trees in class 4 exhibited significantly higher NDVI SD than those in class 1 to 3, indicating greater heterogeneity in canopy reflectance.

Moreover, the CV showed a consistent upward trend from class 1 to class 4, with a statistically significant difference between class 1 and 4. This suggests that, in addition to the observed decrease in NDVI values with increasing disease severity (Fig. 5), the relative variability of NDVI within individual tree crowns becomes more pronounced. While SD reflects the absolute spread of NDVI values, the CV normalizes this spread by accounting for mean differences between trees, thus emphasizing the disproportionate increase in heterogeneity among more severely damaged individuals. Therefore, healthier trees have both higher and more consistent NDVI values, whereas trees suffering from advanced ash dieback show lower NDVI and increased spatial irregularity across their crowns.

Tree crown segmentation in orthophoto

The application of the newly developed workflow for a detailed tree crown segmentation was also successfully applied to an orthophoto generated from a UAV-survey. Despite the lower image resolution due to the flight height of 80 m, individual tree crowns were successfully delineated from their surroundings (Fig. 8). Not only the shape of the tree crowns was replicated but also gaps in the tree crowns (Fig. 8, purple frame), both in large trees and in smaller ash trees with severe damage (Fig. 8, orange frame). However, in cases where trees were in contact to surrounding trees, segmentation often merged them into a single object (Fig. 8, blue frame), highlighting a limitation of the method. These results emphasize the importance of spatial separation between individual trees for the segmentation technique to function reliably.

Discussion

Fine and coarse tree crown masks

A novel workflow for the detailed segmentation of ash tree crowns was developed in this study and successfully applied to multispectral close-up UAV imagery and an orthophoto of trees affected by ash dieback.

The ash trees investigated in this study were located on two ash tree orchards, with generous spacing between individual trees. While this setup provides clear crown outlines, the surrounding vegetation, primarily tall grass and small bushes, adds background complexity. Despite these conditions, both tree crown segmentation methods were able to successfully segment the crowns from their surroundings. Accurate segmentation of green plant material is readily

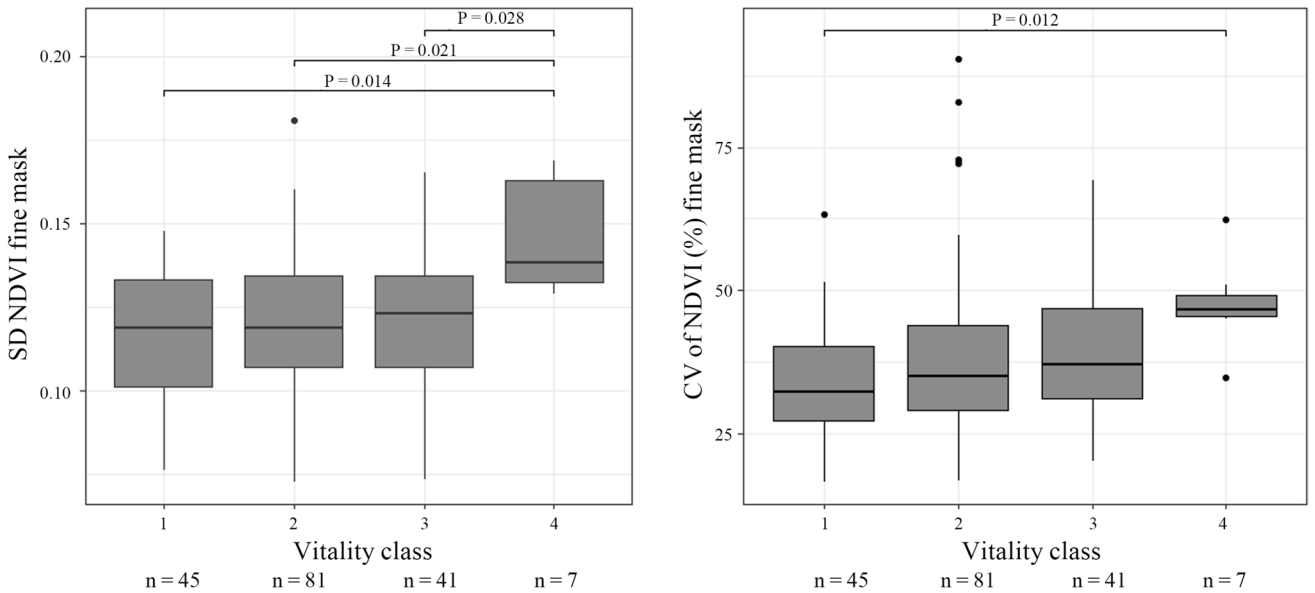

Fig. 7 SD of the NDVI values of the fine mask per vitality class and CV of NDVI of the fine mask per vitality class with significant post-hoc results displayed as bars at the top for the analysed 174 images

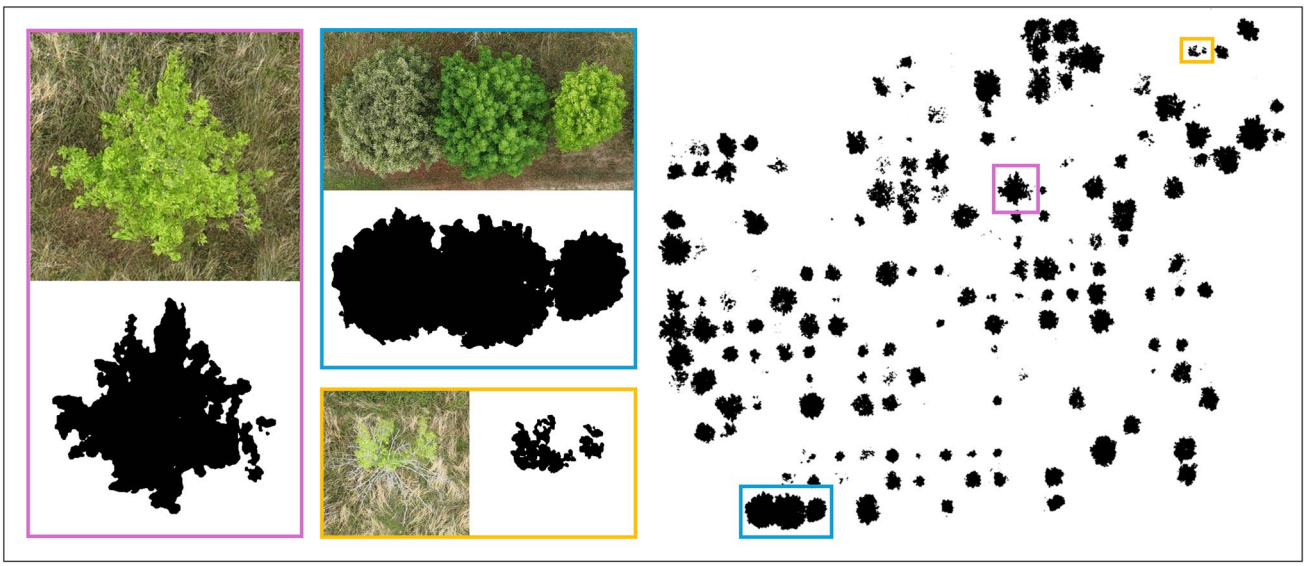

Fig. 8 Segmented tree crowns from an orthophoto with highlighted examples: the crown of a single ash tree (purple frame), detailed images of merged trees (blue frame) and a small, severely damaged ash (orange frame)

achievable when close-up images feature a uniform background. This has been demonstrated among others by Khan et al. (2022), who applied semantic segmentation techniques, and by Wacker et al. (2024), who employed multispectral imaging in combination with chlorophyll fluorescence to enable segmentation. However, as noted by Mishra et al. (2021), segmentation becomes considerably more challenging when the background contains vegetation with similar spectral properties. For instance, while deep-learning models were able to differentiate between crop and weed, difficulties in separating the plant material from the surrounding soil and similar vegetation were reported (Sahin et al. 2023). However, the results of this study demonstrate that successful crown delineation is achievable even in semi-structured environments with vegetation with similar spectral properties.

Many studies on tree crown segmentation rely on remote sensing data acquired from UAVs or satellites (Heenkenda et al. 2015; Zhang et al. 2020; Lassalle et al. 2022). While these datasets often offer relatively high spatial resolution, they frequently lack the detail necessary to capture fine-scale crown structures, such as small canopy gaps, resulting in coarser crown outlines that may not accurately reflect true crown morphology. Only a few studies reported tree crown segmentation results with a level of detail comparable to that achieved in the present study. For instance, LiDAR point clouds have been used to accurately calculate crown volume and segment citrus trees with high morphological accuracy (Liu et al. 2021). Similarly, morphological image analysis applied to multispectral UAV data has enabled detailed crown segmentation in olive orchards (Sarabia et al. 2020), and similar methods were also successfully tested on other orchard species, including lemon and orange trees (Ponce et al. 2022). Additionally, adaptive thresholding combined with watershed segmentation enabled precise delineation of peach tree crowns (Mu et al. 2018). Beyond morphological techniques, deep learning models have shown considerable potential for high-precision crown segmentation. For example, frameworks combining object detection models such as YOLOv4 with LiDAR-derived heightmaps have effectively segmented tree crowns (Sun et al. 2022). UAV-borne LiDAR datasets have been applied across diverse forest types (Chen et al. 2021), and multiple semantic segmentation architectures have been evaluated on multispectral aerial and satellite imagery, further demonstrating the versatility of deep learning approaches for crown segmentation (Ulku et al. 2022).

A key strength of the novel approach developed in our study lies in its ability to segment tree crown areas without the need for annotated training data, making it particularly valuable for large study sites. The combination of spectral and textural indicators—such as NDVI, NIR reflectance, and GLCM-derived metrics—enhances robustness of the method against within-crown variability and background interference. By incorporating edge information and applying unsupervised k-means clustering, the workflow effectively captures the structural heterogeneity commonly observed in high-resolution UAV imagery. The application of k-means clustering in this context has proven to be a viable tool for vegetation or tree crown segmentation, as supported by previous studies. For example, Moussaid et al. (2021) applied k-means clustering to multispectral satellite images of

orchards to segment overlapping tree crowns, successfully distinguishing vegetation from soil and shadows. Similarly, Cinat et al. (2019) compared k-means with other unsupervised methods for segmenting vineyard canopies using UAV-acquired RGB and NIR-Red-Green imagery, demonstrating the applicability of the method in agricultural contexts.

Texture features have been shown to significantly enhance the segmentation and classification of tree crowns. Both Wu et al. (2004) and Erdem and Bayrak (2023) demonstrated that incorporating texture information, ranging from simple image gradients to advanced radiomic descriptors, can improve accuracy in identifying crown boundaries and distinguishing species.

In our novel tree crown segmentation approach, the NIR image and derived NDVI serve as the basis input for all further segmentation steps. The suitability of NDVI and NIR imagery for tree crown segmentation has been consistently demonstrated across multiple studies. Kang et al. (2017) showed that UAV-acquired NIR imagery provided strong spectral contrast between eucalyptus crowns and their surroundings, enabling accurate segmentation. Furthermore, Safonova et al. (2021) highlighted, that models trained on NDVI and GNDVI (Green Normalized Difference Vegetation Index) outperformed those using RGB alone for segmenting olive tree crowns. These studies confirm that NDVI and NIR imagery can enhance crown visibility. Despite these advantages, using the NIR image for segmentation alone can introduce variability due to different illumination conditions, especially in shadowed areas within the crown diminishing visual consistency. Conversely, NDVI by itself often lacks sufficient contrast to clearly distinguish the tree crown from spectrally similar surrounding vegetation. As demonstrated in our study, generating a hybrid image by merging NIR and NDVI data enhances crown delineation. This fusion highlights crown structure while simultaneously reducing the visual impact of shadowed regions and thereby offering a more consistent and robust basis for segmentation.

The UAV close-up images were captured at two study sites from June to October, covering different stages of the vegetation period of the common ash. No differences in segmenting the images were noted for the three analysed months, indicating that the developed segmentation algorithm can be applied to images captured during the entire vegetation period of the common ash. However, as Lu et al. (2022) pointed out, natural illumination can cause shaded and non-shaded areas within individual crowns. These effects were minimized by generating the hybrid NIR-NDVI image in our study. Additionally, a more evenly distribution of shadowed areas can be achieved by performing UAV surveys under overcast conditions, which avoids the harsh contrasts caused by direct sunlight.

Although the SAM model did not capture crown gaps and lacked detail along the crown edges, it was still able to generate tree crown masks that accurately represented the overall crown outline. However, in our study, the SAM model was applied exclusively to individual images of tree crowns, with the crown consistently positioned at the centre of each image. The SAM model was also able to detect and segment tree crowns to analyse changes in riparian woodland (Dawson et al. 2025). Similarly Balasundaram et al. (2024) reported successful background separation of plants using SAM. However, in a comparative evaluation, SAM underperformed relative to three other deep learning models (Speckenwirth et al. 2024). In our study, the SAM model was configured to generate three segmentation masks per ash tree crown. Each mask was manually reviewed, and the most accurate one was selected. However, relying solely on the model's confidence scores would have occasionally led to the selection of an incorrect mask.

Validation of a representative subset of the data revealed a high IoU for both the fine and coarse segmentation masks. However, a closer examination of precision and F1-score metrics indicated that the fine mask more accurately captured the true shape of the tree crowns. These findings suggest that, although both segmentation approaches performed reasonably well in delineating the general crown area, the fine mask provided a more accurate representation of the actual crown structure. This advantage was particularly evident in severely damaged trees, where accurate depiction of remaining leaf mass is critical. Therefore, fine-scale segmentation is strongly recommended in contexts where detailed crown morphology and subtle structural variation are of analytical importance. This distinction proves as particularly important when assessing the health condition of ash trees, where crown size and internal structure serve as key indicators of disease severity. In severely damaged crowns, structural complexity increases due to the emergence of epicormic shoots (Enderle et al. 2015). These dense clusters can partially close crown gaps and create a more heterogeneous crown surface. As a result, the coarse segmentation approach tends to miss fine structural details and underestimates the distribution of living biomass, especially where small, scattered shoots predominate.

Both the development of the fine-scale tree crown segmentation workflow and the application of the SAM model were conducted on very high-resolution images of individual ash trees. To assess the workflow's transferability to coarser spatial scales, its performance was further evaluated on lower resolution orthophotos. Despite the reduced resolution, the segmentation approach, designed to isolate leaf mass, proved effective when applied to an entire ash tree orchard. These results demonstrated the method's scalability and robustness, highlighting its potential for broader application in landscape-level crown analysis. While crown gaps were accurately identified and the reduced leaf mass in severely damaged trees was well captured, cases where tree

canopies overlapped often resulted in a single segmented crown encompassing multiple adjacent trees. This challenge was also observed by Mu et al. (2018) and Sarabia et al. (2020). However, additional processing steps like morphological erosion (Marques et al. 2019) or seed markers from regional maxima and a watershed algorithm (Ponce et al. 2022) can further improve the tree crown masks and separate connecting masks.

NDVI analysis

One of the main objectives of this study was to assess whether delineating only the coarse crown outline is sufficient for calculating mean vegetation index values in severely damaged ash tree crowns. In particular, we examined whether the increasing presence of crown gaps significantly affects these values. While no significant differences in mean vegetation index values were observed between the fine and coarse crown segmentations, the analysis of the difference area, i.e., the part included in the coarse but excluded from the fine mask, revealed substantially lower NDVI values across all vitality classes. This suggests that although the inclusion of ground pixels does not markedly alter the overall mean index when comparing full crown masks, it does introduce a component with clearly lower vegetation activity, particularly reflecting gaps and exposed background beneath sparse crowns.

The observed decline in mean NDVI values with increasing damage due to ash dieback is in accordance with the findings of Buchner et al. (2025), who also reported lower NDVI values in severely damaged ash trees compared to those with only mild symptoms. This decrease in NDVI is explained by the loss of chlorophyll-rich foliage in damaged crowns, leading to reduced reflectance in the NIR spectrum relative to the red spectrum.

The comparison between coarse and fine crown masks revealed notable differences in NDVI variability across vitality classes. While SD of NDVI increased with declining tree vitality, significant differences between mask types were observed particularly in moderately damaged trees (classes 2 and 3). In these cases, coarse masks yielded higher variability, likely due to the inclusion of non-foliar elements such as exposed branches and crown gaps. In contrast, the fine masks, which focused on leaf mass, provided a more consistent and presumably a more biologically relevant measure of canopy composition. The area difference between the fine and coarse masks also increased with damage severity, reflecting the greater inclusion of non-leaf pixels in coarse masks as crown gaps expanded.

The analysis of NDVI variability within in detail segmented ash tree crowns, revealed a consistent increase in heterogeneity in index values with rising damage severity, indicating that NDVI values vary within the crown, especially in trees with severe damage. Similarly, Flynn et al. (2024) documented a spatial pattern in greenness (green chromatic coordinate) decline toward the crown extremities, whereas healthy ash trees, not affected by ash dieback, showed increased greenness at the edges. These results suggest that infection increases within-crown heterogeneity. Accordingly, while mean NDVI values can reliably represent overall crown condition in trees with mild symptoms, they may not fully capture the internal variability of crowns in more severely damaged individuals.

The proposed workflow, designed to account for significant crown gaps in ash trees affected by dieback, proved effective in evaluating the influence of external pixel inclusion on mean vegetation index values and in capturing differences in crown homogeneity across damage classes. Its main limitation lies in the requirement for isolated ash trees without overlapping foliage from surrounding vegetation. However, the workflow offers considerable flexibility, such as adjustable hybrid blending and clustering parameters, making it readily adaptable to other vegetation types and research objectives.

Conclusion

Detailed segmentation of the leaf mass in ash trees affected by ash dieback is feasible and can be applied not only to individual close-range multispectral UAV images but also to orthophotos generated from broader UAV surveys. This novel workflow effectively captures both fine crown edges and internal crown gaps. However, as demonstrated by the comparison between fine and coarse crown segmentation, there was no significant difference in mean vegetation index values per crown, indicating that coarse tree crown segmentation is sufficient for such calculations. Nonetheless, the fine segmentation revealed increasing heterogeneity in NDVI values with greater symptom severity. Therefore, for in-depth crown analysis, particularly when assessing structural integrity or spatial variation in canopy health, the fine segmentation method is recommended. Our approach supports remote, scalable, and reproducible monitoring of forest health, applicable beyond ash dieback and relevant to tree species under similar stressors.

Acknowledgements We thank the Forestry Baden-Wuerttemberg and the Forest Research Institute Baden-Wuerttemberg for providing the seed orchards as study sites. We thank Tobias Heckmann for insightful discussions. Special thanks to all student assistants for their technical assistance.

Funding Open Access funding enabled and organized by Projekt DEAL.

Declarations

Conflict of interest The authors have no relevant financial or non-financial interests to disclose.

References

Agostinelli M, Nguyen D, Witzell J, Cleary M (2021) Mycobiome of *Fraxinus excelsior* with different phenotypic susceptibility to ash dieback. Front Glob Change 4:580514. https://doi.org/10.3389/ffgc.2021.580514

Argamosa RJL, Paringit EC, Quinton KR, Tandoc FAM, Faelga RAG, Ibañez CAG, Posilero MAV, Zaragosa GP (2016) Fully automated gis-based individual tree crown delineation based on curvature values from a lidar derived canopy height model in a coniferous plantation. Int Arch Photogramm Remote Sens Spatial Inf Sci XLI-B8:563–569. https://doi.org/10.5194/isprsarchives-xli-b8-563-2016

Balasundaram A, Sharma A, Kumaravelan S, Shaik A, Kavitha MS (2024) An improved normalized difference vegetation index (NDVI) estimation using grounded *Dino* and segment anything model for plant health classification. IEEE Access 12:75907–75919. https://doi.org/10.1109/ACCESS.2024.3403520

Baral HO, Queloz V, Hosoya T (2014) *Hymenoscyphus fraxineus*, the correct scientific name for the fungus causing ash dieback in Europe. IMA Fungus 5(1):79–80. https://doi.org/10.5598/imafungus.2014.05.01.09

Barbedo JGA (2019) A review on the use of unmanned aerial vehicles and imaging sensors for monitoring and assessing plant stresses. Drones 3(2):40. https://doi.org/10.3390/drones3020040

Buchner L, Eisen AK, Šikoparija B, Jochner-Oette S (2022) Pollen viability of *Fraxinus excelsior* in storage experiments and investigations on the potential effect of long-range transport. Forests 13(4):600. https://doi.org/10.3390/f13040600

Buchner L, Eisen AK, Jochner-Oette S (2024) Effects of ash dieback on leaf physiology and leaf morphology of *Fraxinus excelsior* L. Trees 38(5):1205–1221. https://doi.org/10.1007/s00468-024-02546-1

Buchner L, Eisen AK, Jochner-Oette S (2025) Identification of damage severity in *Fraxinus excelsior* L. trees caused by ash dieback using multisensory and multitemporal UAV imagery. For Ecol Manage 585:122660. https://doi.org/10.1016/j.foreco.2025.122660

Chan AHY, Barnes C, Swinfield T, Coomes DA (2021) Monitoring ash dieback (*Hymenoscyphus fraxineus*) in British forests using hyperspectral remote sensing. Remote Sens Ecol Conserv 7(2):306–320. https://doi.org/10.1002/rse2.190

Chen XX, Jiang K, Zhu YS, Wang XJ, Yun T (2021) Individual tree crown segmentation directly from UAV-borne LiDAR data using the PointNet of deep learning. Forests 12(2):131. https://doi.org/10.3390/f12020131

Cinat P, Di Gennaro SF, Berton A, Matese A (2019) Comparison of unsupervised algorithms for vineyard canopy segmentation from UAV multispectral images. Remote Sens 11(9):1023. https://doi.org/10.3390/rs11091023

Coker TLR, Rozsypálek J, Edwards A, Harwood TP, Butfoy L, Buggs RJA (2019) Estimating mortality rates of European ash (*Fraxinus excelsior*) under the ash dieback (*Hymenoscyphus fraxineus*) epidemic. Plants People Planet 1(1):48–58. https://doi.org/10.1002/ppp3.11

Dalponte M, Reyes F, Kandare K, Gianelle D (2015) Delineation of individual tree crowns from ALS and hyperspectral data: a comparison among four methods. Eur J Remote Sens 48(1):365–382. https://doi.org/10.5721/EuJRS20154821

Dawson M, Dawson H, Gurnell A, Lewin J, Macklin MG (2025) Ai-assisted interpretation of changes in riparian woodland from archival aerial imagery using Meta's segment anything model. Earth Surf Process Landf 50(1):e6053. https://doi.org/10.1002/esp.6053

DJI (2022) DJI Mavic 3M user manual

Douss R, Farah IR (2022) Extraction of individual trees based on canopy height model to monitor the state of the forest. Trees for People 8:100257. https://doi.org/10.1016/j.tfp.2022.100257

Eisen AK, Fussi B, Šikoparija B, Jochner-Oette S (2022) Aerobiological pollen deposition and transport of *Fraxinus excelsior* L. at a small spatial scale. Forests 13(3):424. https://doi.org/10.3390/f13030424

Eisen AK, Semizer-Cuming D, Jochner-Oette S, Fussi B (2023) Pollination success of *Fraxinus excelsior* L. in the context of ash dieback. Ann for Sci 80(1):22. https://doi.org/10.1186/s13595-023-01189-5

Eisen AK, Buchner L, Fussi B, Jochner-Oette S (2024) Does ash dieback affect the reproductive ecology of *Fraxinus excelsior* L.? J for Res 35(1):16. https://doi.org/10.1007/s11676-023-01670-x

Enderle R, Nakou A, Thomas K, Metzler B (2015) Susceptibility of autochthonous German *Fraxinus excelsior* clones to *Hymenoscyphus pseudoalbidus* is genetically determined. Ann for Sci 72(2):183–193. https://doi.org/10.1007/s13595-014-0413-1

Erdem F, Bayrak OC (2023) Evaluating the effects of texture features on *Pinus sylvestris* classification using high-resolution aerial imagery. Ecol Inform 78:102389. https://doi.org/10.1016/j.ecoinf.2023.102389

Flynn WRM, Grieve SWD, Henshaw AJ, Owen HJF, Buggs RJA, Metheringham CL, Plumb WJ, Stocks JJ, Lines ER (2024) UAV-derived greenness and within-crown spatial patterning can detect ash dieback in individual trees. Ecol Solut Evid 5(2):e12343. https://doi.org/10.1002/2688-8319.12343

Freudenberg M, Magdon P, Nölke N (2022) Individual tree crown delineation in high-resolution remote sensing images based on U-net. Neural Comput Appl 34(24):22197–22207

Fuchs S, Häuser H, Peters S, Knauf L, Rentschler F, Kahlenberg G, Kätzel R, Evers J, Paar U, Langer GJ (2024) Ash dieback assessments on intensive monitoring plots in Germany: influence of stand, site and time on disease progression. J Plant Dis Prot 131(5):1355–1372. https://doi.org/10.1007/s41348-024-00889-y

Gross A, Holdenrieder O, Pautasso M, Queloz V, Sieber TN (2014) *Hymenoscyphus* pseudoalbidus, the causal agent of European ash dieback. Mol Plant Pathol 15(1):5–21. https://doi.org/10.1111/mpp.12073

Heenkenda MK, Joyce KE, Maier SW (2015) Mangrove tree crown delineation from high-resolution imagery. Photogramm Eng Remote Sens 81(6):471–479. https://doi.org/10.14358/PERS.81.6.471

Huang HY, Li X, Chen CC (2018) Individual tree crown detection and delineation from very-high-resolution UAV images based on bias

field and marker-controlled watershed segmentation algorithms. IEEE J Sel Top Appl Earth Obs Remote Sens 11(7):2253–2262. https://doi.org/10.1109/JSTARS.2018.2830410

Huete AR (2012) Vegetation indices, remote sensing and forest monitoring. Geogr Compass 6(9):513–532. https://doi.org/10.1111/j.1749-8198.2012.00507.x

Hultberg T, Sandström J, Felton A, Öhman K, Rönnberg J, Witzell J, Cleary M (2020) Ash dieback risks an extinction cascade. Biol Conserv 244:108516. https://doi.org/10.1016/j.biocon.2020.108516

Kampen M, Lederbauer S, Mund J-P, Immitzer M (2019) UAV-based multispectral data for tree species classification and tree vitality analysis. Dreiländertagung der DGPF, der OVG und der SGPF in Wien, Österreich – Publikationen der DGPF (28), pp 623–639

Kang J, Wang L, Chen F, Niu Z (2017) Identifying tree crown areas in undulating *Eucalyptus* plantations using JSEG multi-scale segmentation and unmanned aerial vehicle near-infrared imagery. Int J Remote Sens 38(8–10):2296–2312

Ke YH, Quackenbush LJ (2011) A review of methods for automatic individual tree-crown detection and delineation from passive remote sensing. Int J Remote Sens 32(17):4725–4747. https://doi.org/10.1080/01431161.2010.494184

Kestur R, Angural A, Bashir B, Omkar SN, Anand G, Meenavathi MB (2018) Tree crown detection, delineation and counting in UAV remote sensed images: a neural network based spectral–spatial method. J Indian Soc Remote Sens 46(6):991–1004. https://doi.org/10.1007/s12524-018-0756-4

Khan K, Khan RU, Albattah W, Qamar AM (2022) End-to-end semantic leaf segmentation framework for plants disease classification. Complexity 2022:1168700. https://doi.org/10.1155/2022/1168700

Kirillov A, Mintun E, Ravi N, Mao HZ, Rolland C, Gustafson L, Xiao TT, Whitehead S, Berg AC, Lo WY, Dollár P, Girshick R (2024) Segment anything. In: 2023 IEEE/CVF international conference on computer vision (ICCV). IEEE, Paris, pp 3992–4003

Klesse S, Abegg M, Hopf SE, Gossner MM, Rigling A, Queloz V (2021) Spread and severity of ash dieback in Switzerland–tree characteristics and landscape features explain varying mortality probability. Front for Glob Change 4:645920. https://doi.org/10.3389/ffgc.2021.645920

Langer G (2017) Collar rots in forests of Northwest Germany affected by ash dieback. Balt for 23(1):4–19

Lassalle G, Ferreira MP, La Rosa LEC, de Souza Filho CR (2022) Deep learning-based individual tree crown delineation in mangrove forests using very-high-resolution satellite imagery. ISPRS J Photogramm Remote Sens 189:220–235. https://doi.org/10.1016/j.isprsjprs.2022.05.002

Liu XY, Wang YX, Kang F, Yue Y, Zheng YJ (2021) Canopy parameter estimation of *Citrus grandis* var. longanyou based on LiDAR 3D point clouds. Remote Sens 13(9):1859. https://doi.org/10.3390/rs13091859

Lu ZA, Qi LJ, Zhang H, Wan JJ, Zhou JR (2022) Image segmentation of UAV fruit tree canopy in a natural illumination environment. Agriculture (Basel) 12(7):1039. https://doi.org/10.3390/agriculture12071039

Marques P, Pádua L, Adão T, Hruška J, Peres E, Sousa A, Sousa JJ (2019) UAV-based automatic detection and monitoring of chestnut trees. Remote Sens 11(7):855. https://doi.org/10.3390/rs11070855

Mishra P, Sadeh R, Bino E, Polder G, Boer MP, Rutledge DN, Herrmann I (2021) Complementary chemometrics and deep learning for semantic segmentation of tall and wide visible and near-infrared spectral images of plants. Comput Electron Agric 186:106226. https://doi.org/10.1016/j.compag.2021.106226

Mitchell RJ, Broome A, Beaton JK, Bellamy PE, Ellis CJ, Hester AJ, Hodgetts NG, Iason GR, Littlewood NA, Newey S, Pozsgai G, Ramsay S, Riach D, Stockan JA, Taylor AF, Woodward S (2017) Challenges in assessing the ecological impacts of tree diseases and mitigation measures: the case of *Hymenoscyphus fraxineus* and *Fraxinus excelsior*. Baltic for 23(1):116–140

Mohan M, Silva CA, Klauberg C, Jat P, Catts G, Cardil A, Hudak AT, Dia M (2017) Individual tree detection from unmanned aerial vehicle (UAV) derived canopy height model in an open canopy mixed conifer forest. Forests 8(9):340. https://doi.org/10.3390/f8090340

Moussaid A, El Fkihi S, Zennayi Y (2021) Tree crowns segmentation and classification in overlapping orchards based on satellite images and unsupervised learning algorithms. J Imaging 7(11):241. https://doi.org/10.3390/jimaging7110241

Mu Y, Fujii Y, Takata D, Zheng BY, Noshita K, Honda K, Ninomiya S, Guo W (2018) Characterization of peach tree crown by using high-resolution images from an unmanned aerial vehicle. Hortic Res 5:74. https://doi.org/10.1038/s41438-018-0097-z

Murfitt J, He YH, Yang J, Mui A, De Mille K (2016) Ash decline assessment in emerald ash borer infested natural forests using high spatial resolution images. Remote Sens 8(3):256. https://doi.org/10.3390/rs8030256

Neupane K, Baysal-Gurel F (2021) Automatic identification and monitoring of plant diseases using unmanned aerial vehicles: a review. Remote Sens 13(19):3841. https://doi.org/10.3390/rs13193841

Polk SL, Chan AHY, Cui KN, Plemmons RJ, Coomes DA, Murphy JM (2022) Unsupervised detection of ASH dieback disease (*Hymenoscyphus fraxineus*) using diffusion-based hyperspectral image clustering. In: IGARSS 2022—2022 IEEE international geoscience and remote sensing symposium. Kuala Lumpur, Malaysia. IEEE, pp 2287–2290

Ponce JM, Aquino A, Tejada D, Al-Hadithi BM, Andújar JM (2022) A methodology for the automated delineation of crop tree crowns from UAV-based aerial imagery by means of morphological image analysis. Agronomy 12(1):43. https://doi.org/10.3390/agronomy12010043

Pontius J, Martin M, Plourde L, Hallett R (2008) Ash decline assessment in emerald ash borer-infested regions: a test of tree-level, hyperspectral technologies. Remote Sens Environ 112(5):2665–2676. https://doi.org/10.1016/j.rse.2007.12.011

Qiu L, Jing LH, Hu BX, Li H, Tang YW (2020) A new individual tree crown delineation method for high resolution multispectral imagery. Remote Sens 12(3):585. https://doi.org/10.3390/rs12030585

Safonova A, Guirado E, Maglinets Y, Alcaraz-Segura D, Tabik S (2021) Olive tree biovolume from UAV multi-resolution image segmentation with mask R-CNN. Sensors 21(5):1617. https://doi.org/10.3390/s21051617

Sahin HM, Miftahushudur T, Grieve B, Yin HJ (2023) Segmentation of weeds and crops using multispectral imaging and CRF-enhanced U-net. Comput Electron Agric 211:107956. https://doi.org/10.1016/j.compag.2023.107956

Sarabia R, Aquino A, Ponce JM, López G, Andújar JM (2020) Automated identification of crop tree crowns from UAV multispectral imagery by means of morphological image analysis. Remote Sens 12(5):748. https://doi.org/10.3390/rs12050748

Speckenwirth S, Brandmeier M, Paczkowski S (2024) Treeseg—a toolbox for fully automated tree crown segmentation based on high-resolution multispectral UAV data. Remote Sens 16(19):3660. https://doi.org/10.3390/rs16193660

Peters S, Langer G, Kätzel R (eds) (2021) Eschentriebsterben. Kriterien zur Schadensbonitur an Eschen, 1. Auflage. Fachagentur Nachwachsende Rohstoffe (FNR), Gülzow-Prüzen

Sun CX, Huang CW, Zhang HQ, Chen BQ, An F, Wang LW, Yun T (2022) Individual tree crown segmentation and crown width extraction from a heightmap derived from aerial laser scanning data using a deep learning framework. Front Plant Sci 13:914974. https://doi.org/10.3389/fpls.2022.914974

Tahar KN, Asmadin MA, Sulaiman SAH, Khalid N, Idris AN, Razali MH (2021) Individual tree crown detection using UAV orthomosaic. Eng Technol Appl Sci Res 11(2):7047–7053. https://doi.org/10.48084/etasr.4093

Timmermann V, Børja I, Hietala AM, Kirisits T, Solheim H (2011) Ash dieback: pathogen spread and diurnal patterns of ascospore dispersal, with special emphasis on Norway. EPPO Bull 41(1):14–20. https://doi.org/10.1111/j.1365-2338.2010.02429.x

Timmermann V, Nagy N, Hietala A, Børja I, Solheim H (2017) Progression of ash dieback in Norway related to tree age, disease history and regional aspects. Balt for 23:150–158

Torresan C, Berton A, Carotenuto F, Di Gennaro SF, Gioli B, Matese A, Miglietta F, Vagnoli C, Zaldei A, Wallace L (2017) Forestry applications of UAVs in Europe: a review. Int J Remote Sens 38(8–10):2427–2447. https://doi.org/10.1080/01431161.2016.1252477

Ulku I, Akagündüz E, Ghamisi P (2022) Deep semantic segmentation of trees using multispectral images. IEEE J Sel Top Appl Earth Obs Remote Sens 15:7589–7604. https://doi.org/10.1109/JSTARS.2022.3203145

Wacker K, Kim C, van Iersel MW, Sidore B, Pham T, Haidekker M, Seymour L, Ferrarezi RS (2024) Development of an automated low-cost multispectral imaging system to quantify canopy size and pigmentation. Sensors 24(17):5515. https://doi.org/10.3390/s24175515

Waser L, Küchler M, Jütte K, Stampfer T (2014) Evaluating the potential of worldview-2 data to classify tree species and different levels of ash mortality. Remote Sens 6(5):4515–4545. https://doi.org/10.3390/rs6054515

Wu L, Zhang Y, Gao Y, Zhang YI (2004) Tree crown detection and delineation in high resolution RS image. IEEE Int Geosci Remote Sens Sympos 2004:3841–3844. https://doi.org/10.1109/IGARSS.2004.1369961

Zhang JC, Huang YB, Pu RL, Gonzalez-Moreno P, Yuan L, Wu KH, Huang WJ (2019) Monitoring plant diseases and pests through remote sensing technology: a review. Comput Electron Agric 165:104943. https://doi.org/10.1016/j.compag.2019.104943

Zhang N, Wang YT, Zhang XL (2020) Extraction of tree crowns damaged by *Dendrolimus tabulaeformis* Tsai et Liu *via* spectral-spatial classification using UAV-based hyperspectral images. Plant Methods 16:135. https://doi.org/10.1186/s13007-020-00678-2

Zheng JP, Yuan S, Li WJ, Fu HH, Yu L, Huang JX (2025) A review of individual tree crown detection and delineation from optical remote sensing images: current progress and future